Production of spherical semi-crystalline polycarbonate microparticles for Additive Manufacturing by liquid-liquid phase separation

Stephanie Kloos, Maximilian A. Dechet, Wolfgang Peukert and Jochen Schmidt*

Institute of Particle Technology, Friedrich-Alexander-Universität Erlangen-Nürnberg, Cauerstraße 4, D-91058 Erlangen, Germany
Interdisciplinary Center for Functional Particle Systems, Friedrich-Alexander-Universität Erlangen-Nürnberg, Haberstraße 9a, D-91058 Erlangen, Germany

Authors email address:
stephanie.kloos@fau.de (S. Kloos)
maximilian.dechet@fau.de (M. Dechet)
wolfgang.peukert@fau.de (W. Peukert)
jochen.schmidt@fau.de (J. Schmidt)

* Corresponding author:
Dr. rer. nat. Jochen Schmidt
Tel. +49 9131 8529408
Fax: +49 9131 8529402
Email: jochen.schmidt@fau.de

Publisher's version:

Powder Technology 335 (2018) 275–284
https://doi.org/10.1016/j.powtec.2018.05.005

1. Introduction

Additive Manufacturing (AM), more often simply called “3D-printing”, allows the direct production of solid parts from a three-dimensional CAD model by selective laser sintering (SLS) of powders without the need for any tools or molds. So far, polymer materials available for SLS are very limited [1,2]: preferentially semi-crystalline thermoplasts, in particular polyamide (PA) based powders, are used because of their favorable sintering behavior resulting in devices of good mechanical part properties [1,2]. Besides PA12, PA11 and PA6, some niche products such as polystyrene (PS), polypropylene (PP), polyethylene (PE), thermoplastic polyurethane (TPU) und polyether ether ketone (PEEK) are available [1–3].

Polycarbonate (PC) is well-known for its high toughness (it has a higher impact resistance than PEEK), good thermal stability and flame resistance [4]. Thus, PC powders of optimized processability are of great interest for additive manufacturing of functional parts by SLS. Especially blends of PC with another thermoplast [5–8] will allow for improved mechanical properties [9]. Amorphous PC for rapid prototyping applications is commercially available as DTM Laserlite Polycarbonate Compound LPC3000 laser sintering powder and as Grade S1438 from BFGoodrich Co. These amorphous PC powders consist of irregular shaped particles [10–12] which is typical for polymer powders produced by top-down approaches like cryogenic (dry) grinding [13,14] or wet grinding [15–19]. Irregular shaped particles may lead to poor SLS processability and inferior mechanical part properties. Moreover, when dealing with amorphous materials, the building chamber temperature in the SLS process is limited to the glass transition temperature T_g. Due to the amorphous nature of the so far available PC powders, their application is limited to the manufacture of devices, where the mechanical part properties and dimensional accuracy were of minor importance, e.g. in investment casting. Thus, the development of novel semi-crystalline PC powder systems would allow for higher building chamber temperatures and the utilization of the so-called a thermal ‘sintering window’. The temperature range between solidification temperature and melting temperature is most relevant since a higher building chamber temperature will reduce issues with so-called curling, i.e. the liftoff of the part edges due to differences in shrinkage. Curling is a major reason for parts of minor quality, i.e. dimensional inaccuracy or inferior strength.

To further extend the applications of SLS, in addition to the optimization of SLS devices, e.g. in terms of the powder spreading process, new powders with improved powder properties must be developed. Powder properties, SLS processability and the resulting part properties are directly connected [17,20–22]. In particular, high packing densities and good powder flowability are key parameters towards good processability and part properties (c.f. mechanical strength, dimensional accuracy). Flowability and packing density can be tailored by proper choice of particle size, shape and surface roughness. Besides spherical shaped powders [17,19,20,23–26] of narrow size distribution functionalized with flowing aids [21,22]

also slightly elongated particles proved to be feasible in terms of flowability and packing density: actually, powders made up of spherocylindrical particles of an aspect ratio of 1.5 [27,28] show a higher bed density as compared to a particle system made up of spheres.

The bed quality, i.e. the packing density of the powder bed and the surface roughness is not only a function of particle characteristics but depends also on the used mode of powder spreading. Typically blades or counter-rotating roller coaters are used [1,2]. Recent DEM studies enabled deeper insights into the powder spreading process. For example, a roller coater outperforms a blade under comparable conditions with respect to a higher bed density [28] and broader particle size distributions may lead to powder layers of higher porosity [28,29]. Moreover, it could be shown that the optimization of the blade geometry allows to significantly improve the bed density for irregular particles [30].

Recently, two scalable approaches for the production of spherical polymer microparticles of good flowability comprising top-down processes have been proposed [25]: In the first approach the process chain [17,19] consists of the consecutive steps cold wet grinding [7,15,18,19], rounding of the produced irregular shaped cohesive particles in a heated downer reactor [24,26], and a final dry coating step [22,31,32] for optimized flowability. The second approach, melt emulsification, allows to obtain polymer particles in a single process step at the expense of more complex processing equipment. Here, the polymer is molten and polymer droplets are produced by shear and elongational stress using a rotor-stator device. Upon cooling of the melt emulsion, spherical particles are obtained. Besides these methods, precipitation, thermally induced phase separation (TIPS) and co-extrusion have been proposed for the production of spherical SLS powders [1,2,23,33,34]. In the case of PA12, TIPS has been demonstrated to be feasible for powder production in a batch process at industrial scale (2 … 3 m^3) [35–37].

Within this contribution thermally induced phase separation in cyclohexanol is discussed as a promising, straightforward single-step approach for the production of semi-crystalline spherical PC microparticles of good flowability starting from amorphous injection moulding grade PC feed material. The obtained PC microspheres are characterized with respect to powder properties and structural characteristics using laser diffraction particle sizing, scanning electron microscopy (SEM), Raman spectroscopy, differential scanning calorimetry (DSC) and X-Ray diffraction (XRD). The powder's processability in SLS was assessed by flowability measurements using a tensile strength tester [38,39], powder deposition experiments [17,22] and sintering of single layer specimen. The flowability of the obtained spherical PC particles was optimized by dry coating with fumed silica. Dense layers are obtained confirming the correlation between powder flowability and part properties [17,20,22].

2. Thermally induced phase separation

Thermally induced liquid-liquid phase (TIPS) separation in ethanolic environment is a well-known method for the production of PA12 particles for SLS [35–37]. There, the supersaturation necessary to trigger phase separation and consecutive precipitation of the solid typically is realized by cooling and subsequent evaporation of the solvent. The product particle size distribution (PSD) depends on the stirrer speed and the temporal temperature profile. Apart from SLS applications, liquid-liquid phase separation has been reported for several polymers, although, to the best of our knowledge, TIPS has not yet been reported as an approach for production of semi-crystalline PC microspheres. For example, Nichols et al. [34] describe the formation of spherical polybutylene terephthalate (PBT) particles by crystallization from solution by a liquid-liquid phase separation process using epoxy resin as solvent. Garber and Geil [40] addressed the formation of poly-3,3-bis(chloromethyl)-oxacyclobutane (BCMO) “globules”. The aforementioned process was investigated for polyethylene by Schaaf et al. [41] and Hay and Keller [42], for polypropylene by Wang et al. [33]. Liquid-liquid phase separation for nylon polymers was investigated by Hou and Lloyd [43], while Blaker et al. [44] addressed poly(lactide-co-glycolide). Thermally induced liquid-liquid phase separation typically is applied for the production of porous membranes [45–47] and scaffolds [48,49].

The phase diagram of a polymer in a poor solvent (binary system) as described by Richards [50] and Flory [51] is given schematically in Figure 1 for a monodisperse polymer: At high temperatures the polymer is completely dissolved in the solvent; i.e. the solution is homogeneous and stable. By cooling (or quenching) below a critical temperature the solution becomes unstable and liquid-liquid phase separation into a solvent-rich and a polymer-rich phase occurs. Phase separation frequently is accompanied by the occurrence of turbidity due to the formation of droplets, when crossing the binodal (coexistence curve). In the region between the binodal (c.f. solid line in Figure 1) and the spinodal (dotted line) the system is metastable. Phase separation into a polymer-rich and a solvent-rich liquid phase occurs and a dispersed system is formed. At low polymer concentrations the polymer-rich liquid phase is the dispersed phase and at moderate cooling rates particles are formed by nucleation and growth. At high polymer concentrations the continuous phase is the polymer-rich phase and membranes are obtained upon cooling. By rapid cooling to temperatures below the spinodal, spinodal decomposition occurs and two co-existing phases are formed, which results in the formation of microporous interconnected structures. While the system is liquid, coarsening effects like coalescence and Ostwald ripening can occur due to the tendency of the system to reduce its interfacial free energy [45,52,53].

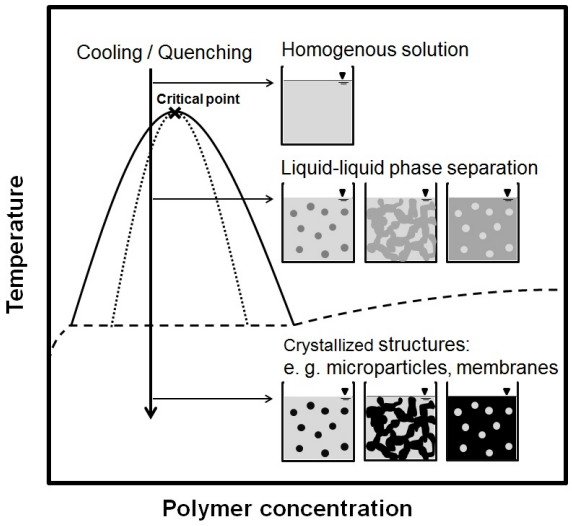

Figure 1: Schematic phase diagram for a polymer solution with a miscibility gap: structure formation by temperature induced phase separation, adapted from Richards [50], Flory [51], Schaaf [41], Tsai and Torkelson [45], van de Witte et al. [54], Wang [33]; ─ binodal, ···· spinodal, - - crystallization temperature.

3. Materials and methods

3.1 Materials

Ground PC (< 0.5 mm size) was obtained by comminution of Bisphenol-A based amorphous polycarbonate Makrolon®2405 (Covestro), provided as granules of approximately 4 mm size. The glass transition temperature of the polymer was 144°C. Comminution was performed in a rotary impact mill Pulverisette-14 (Fritsch) equipped with a pin rotor operated at n_P = 20000 min^{-1} and a sieve ring (0.5 mm). The granules were pre-cooled with liquid nitrogen prior to comminution; a mean product particle size of $x_{50,3}$ ≈ 194 µm was obtained. The particle size distribution (PSD) measured by laser diffraction particle sizing and a SEM image of the ground material are depicted in Figure 2. Cyclohexanol (Merck) was used as solvent in the TIPS process. Fumed silica (Evonik Industries) was applied as flowing aid.

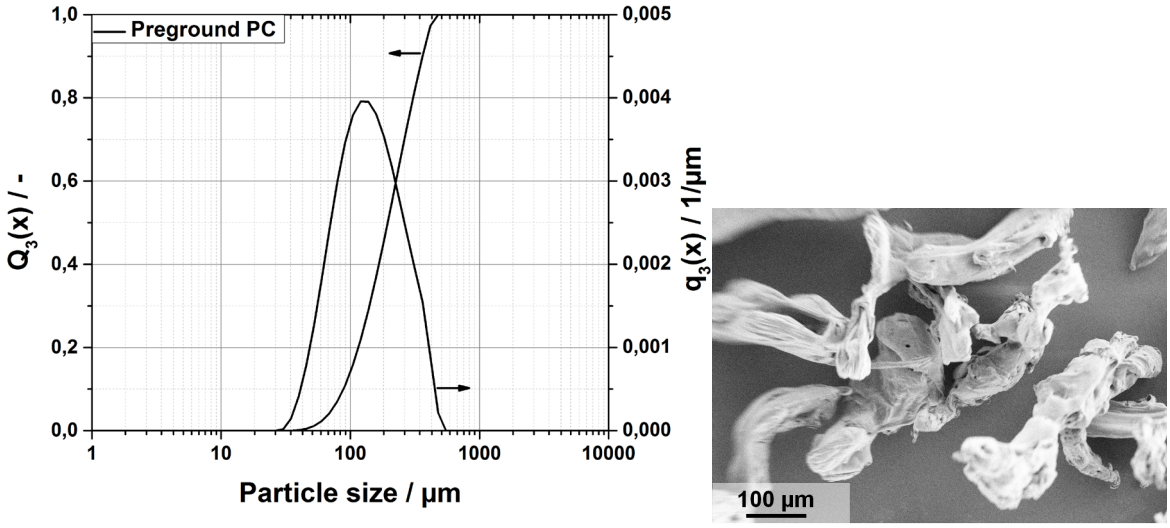

Figure 2: Particle size distribution (volume, density q_3 and cumulative Q_3) and SEM image of the pre-ground PC feed material.

3.2 Experimental setup

Teflon-lined autoclaves DAB-3 (Berghof) with a maximum volume of 250 mL, which can be operated at a maximum temperature of 250°C and a maximum pressure of 200 bar, were used in liquid-liquid phase separation experiments. A typical batch mass (solvent + polymer) was around 40 g. The autoclaves were placed on hot plates within heating blocks. The heating block temperature was controlled by NiCr-Ni thermocouples (type K). The difference between set and actual temperature at stationary conditions typically was less than 3 K. The process temperatures reported in the following refer to the temperatures measured in the heating blocks, which are assumed to be very close to the temperature inside the autoclaves. The autoclaves were equipped with PTFE-coated magnetic bars of 6 mm diameter and 25 mm length to allow for stirring. Experiments have been performed with stirrer speeds in the range between 0 rpm and 1250 rpm. In all experiments the autoclaves were allowed to cool to room temperature in the laboratory atmosphere, resulting in rather small cooling rates in the range from 0.5 to 3 K/min, see Figure S-1. In the first test series referred to as ‘cooling without stirring’ the stirrer and the heating were stopped at the same time and the autoclaves were allowed to cool. In the second test series ‘cooling with stirring’ the stirrer was operated at a reduced speed of 250 rpm during cooling. The obtained product particles were washed with ethanol, separated from the liquid phase by centrifugation, and dried at slightly elevated temperature (approx. 60°C).

Dry particle coating of the PC microparticles was performed using a tumbling mixer (T2F, Willy A. Bachofen AG) operated at 72 min^{-1} for 10 minutes. A mass concentration of around 1

% of silica with respect to polymer host particles has been applied. For details on the dry coating of polymers and its influence on flowability, please refer to our previous work [19,22].

3.3 Characterization methods

3.3.1 Laser diffraction particle sizing

Laser diffraction particle sizing with a Mastersizer 2000 equipped with a Hydro 2000S wet dispersion unit (Malvern) was used to measure the PSDs of the product particles. The dried product was re-dispersed in water applying ultrasonication. Sodium dodecyl sulphate (SDS, 98 %; Merck) was added to enhance wettability and to improve dispersibility of the polymer particles. Within the wet dispersion unit the suspensions have been diluted as appropriate with deionized water prior to measurement.

3.3.2 Scanning Electron Microscopy (SEM)

Particle shape and surface morphology were characterized by scanning electron microscopy (SEM) with a Gemini Ultra 55 (Carl Zeiss) operated at an acceleration voltage of 1.0 kV. A through-the-hole detector was used for imaging.

3.3.3 Cloud point determination

The cloud point curve was determined for PC concentrations up to 5 wt-% similar to the procedure proposed in [55]. First, the polymer was dissolved in cyclohexanol in a beaker by heating the system to 158°C using a hot plate with magnetic stirrer. After a transparent solution was obtained, the heating was switched off and the system was allowed to cool down slowly. The cloud point was determined visually as the temperature, where the transparent solution turned turbid. The transition to the turbid system is easily detected by eye. The cloud point temperatures reported below are the average of three single determinations. Temperatures were monitored by type K thermocouples with an accuracy of around 2 K.

3.3.4 Raman spectroscopy

Spectra were collected with a LabRAM HR Evolution Raman spectrometer (Horiba) equipped with a frequency-doubled Nd-YAG laser (λ = 532 nm; grating 1800 gr/mm; 50 x LWD objective) for Raman shifts between 100 cm^{-1} and 3200 cm^{-1}. For sample preparation, dispersions were deposited on a glass sample holder by drop coating and the dispersion was allowed to dry at 40°C.

3.3.5 Differential scanning calorimetry (DSC)

Differential scanning calorimetry (DSC) was performed with a DSC8000 (PerkinElmer). The samples were placed in standard aluminum pans with covers and measured at a heating rate of 80 K/min from 30°C to 270°C followed by cooling to 30°C at 10K/min under nitrogen purge gas flow (25 mL/min). The temperature cycle was performed two times. The crystallinity X_c of the polymer samples was calculated from the experimentally determined heat of fusion according to equation 2:

(eq.2) $$X_c = \frac{\Delta H_f}{\Delta H_f^0} \cdot 100\%$$

ΔH_f is the measured melting enthalpy and ΔH_f^0 is the melting enthalpy of fully-crystalline PC material. A value of ΔH_f^0 = 26 cal/g (109 J/g) was used for evaluation [56].

3.3.6 X-ray diffraction (XRD)

XRD was performed with a Bruker AXS D8 Advance diffractometer in Bragg-Brentano geometry. The device was equipped with a VANTEC-1 detector and a Ni filter; Cu K_α-radiation (154 pm) was used. The powder samples were prepared in PMMA sample holders. Measurements were done at a step size of 0.014° and a measuring time of 1 s per step in the range 10°≤ 2θ ≤ 90°.

3.3.7 Powder flowability, deposition and sintering of thin layers

The powder flowability was investigated with a modified Zimmermann tensile strength tester [38,39]. The device allows the measurement of adhesion forces between adjacent powder layers in a nearly uncompacted powder bed, i.e. under load conditions comparable to SLS. Experiments were performed at a maximum load of 153 Pa. Further details on the measurement procedure can be found in the literature [19]. The powder deposition behavior was studied by doctor blading with a film applicator device (Coatmaster 510, Erichsen) equipped with a quadruple film applicator Model 360 (gap size 120 µm, coating velocity 100 mm/s). The applied procedure is described in detail elsewhere [17,19,22] as a model experiment for the powder deposition in the SLS process. In short, the substrate's coverage with particles is evaluated, which allows an assessment of the powder deposition behavior. Moreover, single layers were produced with a laser sintering machine M1 cusing (Concept Laser) equipped with a CO_2 laser. Experiments were performed at room temperature at a laser power of P = 20 W and a focus diameter of D_{Laser} = 0.2 mm. The scan speed v_{Laser} was

varied from 400 to 1000 mm/s resulting in laser energy inputs (with respect to illuminated area) of 0.63 J/mm² to 1.57 J/mm² as calculated by equation 3.

(eq.3) $$E = \frac{4 \cdot \pi \cdot P}{D_{Laser} \cdot v_{Laser}}$$

4. Results and Discussion

4.1 Influence of process conditions on particle size distribution and morphology

In this study the influence of the stirring speed, the maximum process temperature and the polymer concentration on size and morphology of PC product microparticles obtained by TIPS was assessed. The influence of the process temperature on the product particle size is summarized in Figure 3 for a PC-cyclohexanol system at 1 wt% polymer concentration. The process time at the respective maximum process temperature was 15 minutes for all experiments. With increasing maximum process temperature from T ≈ 165°C to T ≈ 240°C the particle size gradually increases and remains nearly constant above 210°C (for PSD of product particles obtained at T ≈ 240°C, see Figure 3, right). Obviously a process temperature of 144°C must be exceeded to allow for complete conversion of the feed material: although the polymer starts to dissolve and small particles are formed by thermally induced liquid-liquid separation (c.f. $x_{10,3}$ (T ≈ 144 °C), Figure 3, left), the pre-ground material did not dissolve completely at the chosen conditions as confirmed by SEM imaging (Figure S-3, supporting information). Besides spherical product particles of 3…4 µm size, also non-spherical large particles of similar habitus like the feed material are found.

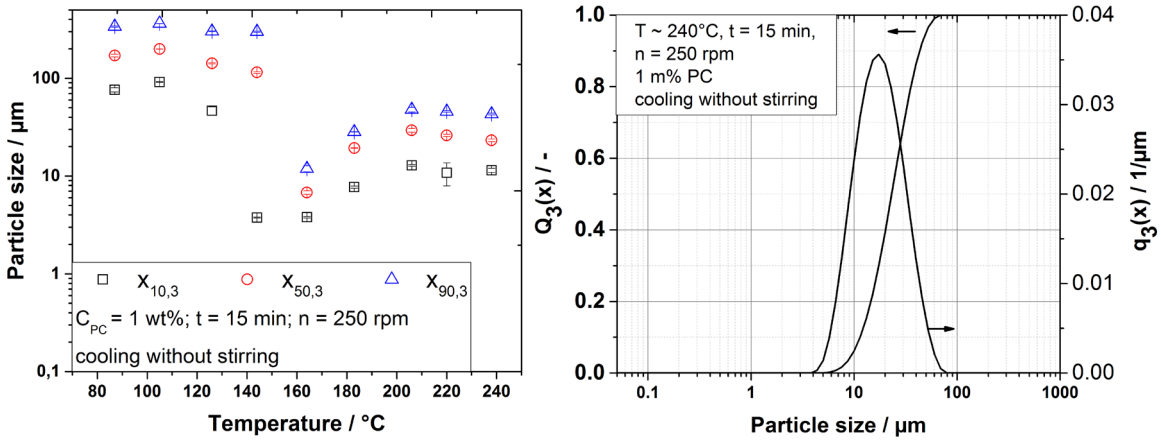

Figure 3: Left: influence of process temperature on the particle sizes $x_{10,3}$, $x_{50,3}$ and $x_{90,3}$; Right: Particle size distribution (volume, density q_3 and cumulative Q_3) of polycarbonate particles produced at T ≈ 240°C, n = 250 rpm.

To get a deeper understanding of the temperature dependencies found, the liquid-liquid-phase separation process was conducted for temperatures up to 158°C in an experimental setup (see section 3.3.3) that allowed for visual inspection. The characteristic temperatures for the process, namely the temperature for complete dissolution of the polymer and the temperature, where liquid-liquid phase separation occurs, i.e. the cloud point, are summarized in Figure 4 for PC concentrations up to 5 wt-%. Depending on the polymer concentration, complete dissolution of the polymer was accomplished at temperatures of 144°C to 148°C (c.f. black squares). Thus, the process temperature has to exceed these aforementioned temperatures to allow for complete conversion of the feed. The observed temperature range is close to the glass transition temperature T_g of polycarbonate. A remarkable increase of polymer solubility when exceeding the glass temperature is well-known. The cloud point temperatures found when slowly cooling the system from the maximum process temperature of around 158°C were found to increase with increasing polymer concentration from 133°C (0.1 wt-%PC) to 147°C (5 wt-% PC). The same behavior of the cloud point temperature on the polymer concentration was observed e.g. also for liquid-liquid phase separation in PP and PLLA systems [33,55].

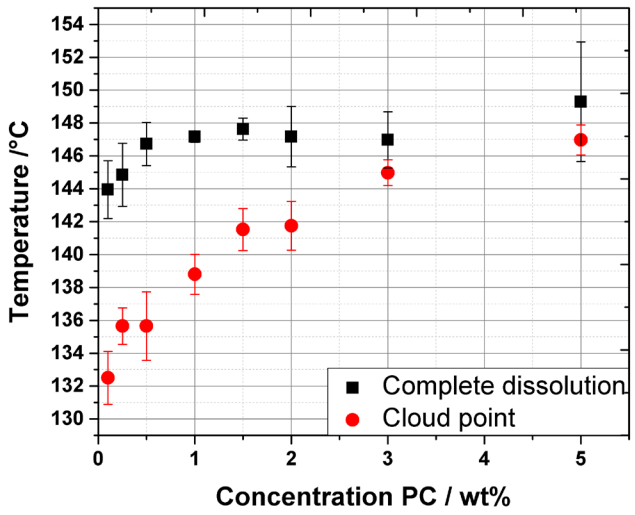

Figure 4: Influence of PC concentration on the temperature, where complete dissolution of the polymer was recognized (black squares) and the cloud point curve (red circles).

The influence of the stirring speed on the PC product particle sizes $x_{10,3}$, $x_{50,3}$ and $x_{90,3}$ is depicted in Figure 5 for a PC cyclohexanol system with a polymer concentration of 1 wt-%. The polymer solution was kept for 15 minutes at the maximum temperature of 240°C and

then was allowed to cool with, respectively, without stirring. Details on the temporal evolution of the process temperature are given in Figures S-1 and S-2 in the supporting information. For these conditions stirring reduces the product particle size from $x_{50,3}$ = 25.0 µm (n = 0 rpm) to 14.8 µm (n = 1250 rpm) in the case of cooling without stirring (Figure 5, left), respectively, to 10.9 µm in the case of stirring during cooling (Figure 5, right).

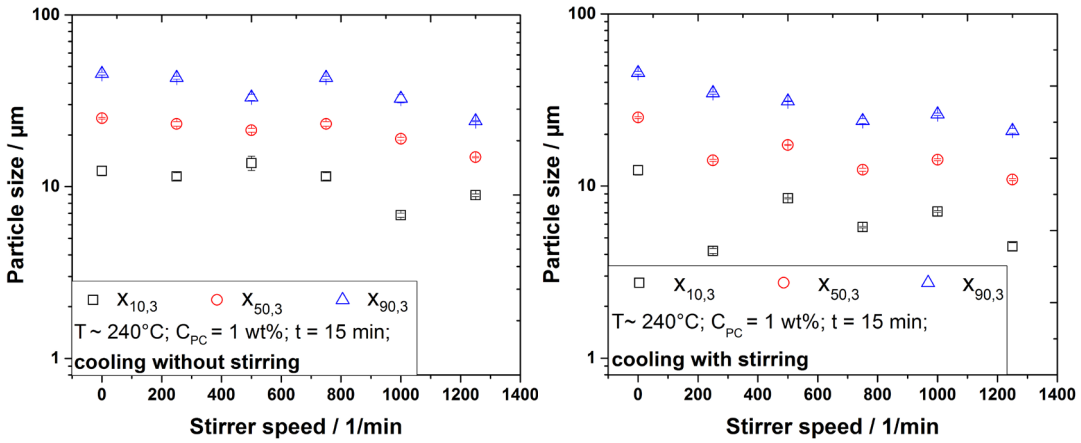

Figure 5: Influence of the stirring speed on the product particle sizes $x_{10,3}$, $x_{50,3}$ and $x_{90,3}$ (1 wt.-% PC, T = 240°C). Left: cooling without stirring, right: cooling with stirring (n = 250 rpm).

Remarkably, the obtained polymer particles are smaller than the currently used commercial laser sintering powders with typical sizes $x_{50,3}$ between 50 and 60 µm. Smaller product particles offer advantages with respect to higher precision of the contours and a lower surface roughness of SLS parts [57]. Good processability of fine polymer powders like polybutylene terephthalate (PBT) with $x_{50,3}$ ≈ 19 µm or polypropylene (PP) with $x_{50,3}$ ≈ 22 µm has been already demonstrated previously [17,23]. With respect to the width of the PC product particle size distributions, as expressed by the span $(x_{90,3} - x_{10,3}) / x_{50,3}$, larger spans between 1.3 and 2.2 were observed for cooling with stirring as compared to spans between 0.9 and 1.4 when cooling without stirring applied: Stirring during cooling may induce breakup of the polymer-rich domains formed during phase separation into smaller droplets and, thus, upon further cooling may lead to smaller crystallized particles.

For production of polyamide powders by liquid-liquid phase separation similar dependencies on the influence of the stirrer speed on the particle size were reported [35,37]. Also Feng et al. [58] and Nie et al. [59] confirmed that when increasing the stirring speed, first a decrease in particle size is found for poly(L-lactic acid) (PLLA) nanofibrous hollow microspheres produced by a combination of phase inversion emulsification and thermally induced phase separation. However, when further increasing the stirring speed, Nie et al. [59] observed an

increase in particle size. The dependency between stirring intensity and particle size is complex and governed by two opposing effects, namely size reduction by droplet breakup (due to stirring and mixing) and coarsening phenomena. The former depends on droplet size, concentration, colloidal stability and prevailing flow patterns in the reactor. Coarsening, i.e. coalescence and Ostwald ripening, is well known for droplets formed by phase separation due to the tendency to reduce the interfacial free energy in the system [52–54]. Thus, we assume a comparable behavior of the phase separated system to emulsions, where the product droplet sizes depend as well on the interplay of ripening and droplet breakup [60]. Ripening phenomena are complex and depend on various system characteristics. For example, droplet ripening is dependent on the droplet size distribution and the mixing intensity [23,60]. Crist and Nesarikar [52] reported that the coalescence of polymer droplets is reduced using a matrix phase with high molecular weight and viscosity. Moreover, Ostwald ripening is reduced in the case of droplets with poor solubility in the matrix phase and a low diffusion coefficient (high molecular weight) [52]. In liquid-liquid phase separation an increase in product particle size was reported for an increase of dispersed phase concentration and a decrease in quenching temperature (c.f. smaller cooling rate) [52,61]. Obviously in our case the effect of size reduction (droplet breakup with increased stirring) dominates the ripening by coalescence, which overall leads to a reduction of product particle size with increased stirring.

For characterization of particle shape and surface morphology SEM imaging was applied. Almost spherical PC particles with nanostructured surfaces were obtained by TIPS at low polymer concentration (1 wt%), see Figures 6 a and 6 b. Thus, good flowability of the powder is expected (see Section 4.3). The nanostructured surface also is a hint for the crystallinity of the particles, which is detailed in section 4.2. The influence of polymer concentration (variation between 1 wt% and 50 wt%) on the product habitus was assessed as well: Whereas for a polymer concentration of 1 wt% spherical particles are formed, with increasing PC concentration the particles gradually become non-spherical. For example, larger cauliflower shaped particles were obtained for c_{PC} = 3wt% (see Figure 6 c). These structures resemble aggregates formed from smaller primary particles. The formation of smaller primary particles with increased polymer concentration can be understood from classical nucleation theory as an effect of a higher supersaturation in the system. The formation of larger product particles with increasing polymer concentration has been reported by Smolders et al., Matsuyama et al. and Wang et al. [33,61,62] as well, although, they did not mention that the larger particles were non-spherical aggregate-like structures. Upon further increase of the polymer concentration from $c_{PC} \approx 5$ wt% the mechanism of the solid formation (c.f. Figure 1) seems to change: instead of isolated particles a porous membrane structure (see Figure 6 d) is obtained [54,61].

FIGURE 6

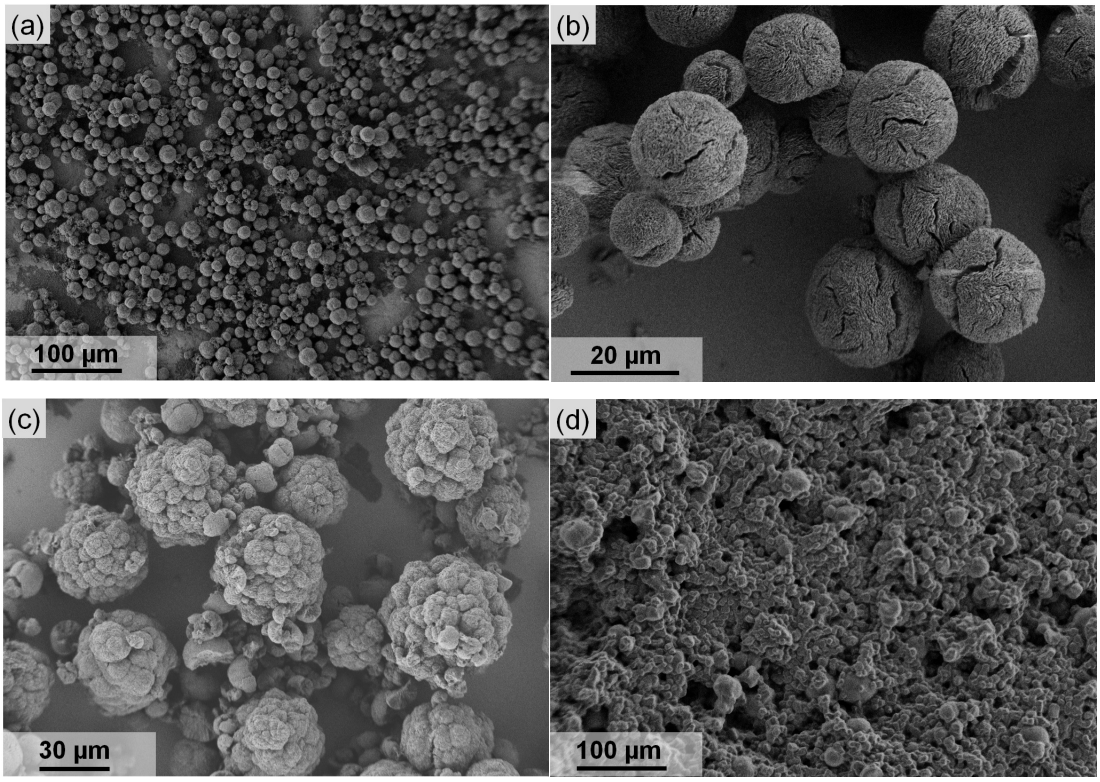

Figure 6: SEM images of polycarbonate micro structures obtained by TIPS – influence of polymer concentration: (a) 1 wt% PC (overview), spherical particles, (b) 1 wt% PC (detail), spherical particles, (c) 3 wt% PC: cauliflower-shaped particles, (d) 20 wt% PC: porous membrane.

4.2 Structural characterization of the PC particles

Besides particle size distribution and shape, which will mainly influence the SLS processability with respect to powder flowability and powder packing, also structural features of the polymer, like its degree of crystallinity, are of immanent importance for the SLS process and the part quality. Thus, dynamic scanning calorimetry (DSC), Raman spectroscopy and XRD were applied for structural characterization of the produced polymer microparticles. Figure 7 (left) shows DSC thermograms of PC particles produced at T ≈ 240°C, n = 250 rpm and cooling without stirring. The typical melting temperature T_m = 224°C of semi-crystalline PC was found [63,64]. Thus, remarkably the proposed TIPS process allows production of semi-crystalline PC microparticles from an amorphous feed material. Presumably, the crystallization is triggered by the presence of cyclohexanol. Crystallization of PC induced by solvents [65], solvent vapors (e.g. acetone) [63,66–69], plasticizers [56,70], supercritical CO_2 [71–73] or stretching [74] has been reported. Solvents or solvent vapors permeate the polymer network promoting rearrangement of the polymer chains (induced crystallization) [75]. In the considered system the formed polymer-rich droplets contain

residual cyclohexanol, which increases the mobility of the polycarbonate chains facilitating reorientation to the thermodynamically favorable crystalline state during solidification. While during the first heating step, crystalline structures in the obtained PC particles are molten, no re-crystallization occurs during cooling: no melting point is observed in the second heating step. The glass transition temperature T_g of the product particles was found to be around 140°C, i.e. somewhat lower than for the PC feed (144°C). During the first temperature cycle the product particles have been transformed into amorphous PC. This observation is confirmed by previous studies; PC is 'hard to crystallize' by thermal treatment and is known to show very slow crystallization kinetics. Hundreds to thousands of hours of isothermal treatment are necessary until remarkable amounts of crystalline polymer are found [64,70,76]. This is another confirmation that the observed crystallization of PC is solvent-induced, as it cannot be triggered solely by the thermal treatment under the process conditions that apply. The reduction of the glass transition temperature could be due to a slight reduction in molar mass of PC during processing. According to Fox and Flory [77] the glass transition temperature is directly proportional to the molar mass. The crystallinity X_c for PC particles produced at different temperatures (see Table 1) was calculated assuming a heat of fusion of fully crystalline PC of ΔH_f^0 = 109 J/g [56] according to equation 2. Depending on the processing conditions of PC, typically crystallinities between 20 % and 40 % - up to values of 62% - are observed [56,63,64,67,71,72,78–80]. In the considered TIPS process, degrees of crystallinity between 18 % (T ≈ 240 °C) and 34 % (T ≈ 165 °C) were found, i.e. the choice of the maximum process temperature allows to tailor semi-crystallinity of the PC microparticles to a certain extend. The different crystallinities are triggered by different cooling rates: With increasing maximum temperature the system initially cools faster and, thus, different cooling rates apply, which will influence the crystallization kinetics. The temporal evolution of temperature in dependency on the maximum process temperature is given in the supporting information, Figure S-1.

Semi-crystallinity of the polymer product particles is proven by XRD (Figure 7, right) as well; sharp diffraction reflexes at 2θ = 17.2° and 2θ = 25.2° being typical for crystalline PC are observed [63,72–74,79–81]. In comparison, the pre-ground feed material shows an XRD pattern typical for amorphous PC, i.e. the crystallinity is induced during the production of the particles in the liquid phase [74,81].

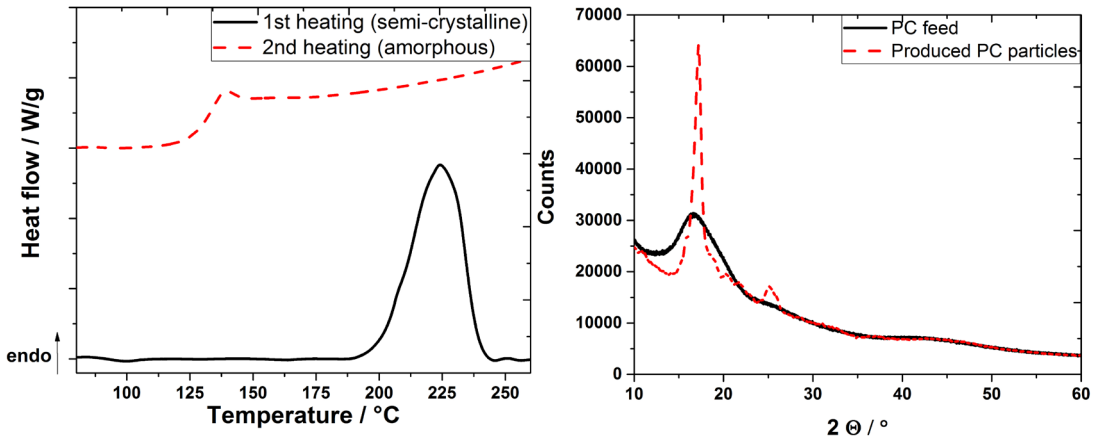

Figure 7: Analysis of the semi-crystalline behavior of the produced PC particles (T ≈ 240 °C, n = 250 rpm, cooling without stirring): thermogram of spherical PC product particles (left) and respective XRD pattern in comparison to the pre-ground amorphous feed material (right).

Table 1: Degree of crystallinity of polycarbonate product particles as determined by DSC.

T / °C	165	185	205	220	240
Crystallinity X_c	34 %	32 %	28 %	23 %	18 %

Crystalline and amorphous PC can be discriminated using Raman spectroscopy as well. Figure 8 depicts Raman spectra of PC feed material ('PC feed'), PC product microparticles obtained by TIPS ('produced PC particles') and 'heated PC particles', i.e. polymer recovered after two DSC heating cycles (30 … 270°C, see above). Significant shifts in peak positions due to the presence of ordered structures in the produced PC particles are observed. The carbonyl band shifts from 1775 cm^{-1} to 1767 cm^{-1}; the broad stretching vibration of the C-O-C group in amorphous PC shifts from 1235 cm^{-1} to 1248 cm^{-1} with a visible shoulder at 1237 cm^{-1} and 1220 cm^{-1} and the C-H out-of-plane bending mode shifts from 735 cm^{-1} to 728 cm^{-1} [80,82]. Upon heating of the produced PC particles (c.f. 'heated PC particles'), the Raman spectrum lacks all of the above described band shifts, which indicates that the fully amorphous structure observed for the PC feed material is formed by heating again, which is in accordance with the DSC analysis.

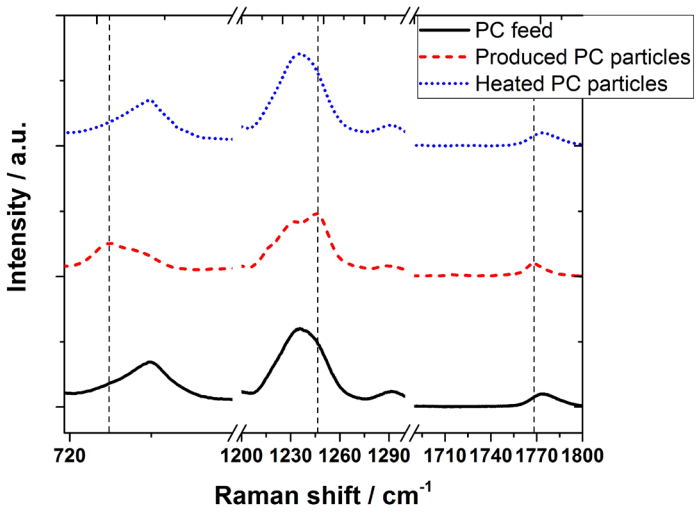

Figure 8: Raman spectra of PC feed material, produced micro particles and heat-treated microparticles.

Due to the thermal characteristics, an improved SLS processability of the novel semi-crystalline PC microparticles is expected: compared to amorphous PC, the semi-crystalline PC particles will allow a higher building chamber temperature in SLS due to the thermal 'sintering window', i.e. the temperature range between solidification temperature and melting temperature is not present in completely amorphous polymers and only can be utilized in the case of semi-crystalline thermoplasts. A higher building chamber temperature in SLS will reduce issues with so-called curling, which is one major reason for parts of minor quality with respect to e.g. dimensional accuracy or strength. Results of DSC and Raman spectroscopy suggest that parts produced by SLS from the semi-crystalline PC powder will be amorphous due to the thermal cycles (melting of the powder and subsequent solidification) they experience during processing.

4.3 Powder flowability, deposition and sintering of thin layers

Tensile strength of powders was measured to assess the powder flowability. Good flowability corresponds to low tensile strength; the interparticulate forces are low and adjacent powder layers can be separated easily. The spherical PC microparticles (T ≈ 240°C, n = 250 rpm, cooling without stirring) show a tensile strength of about 3.5 Pa; after dry coating of the PC microspheres with fumed silica a tensile strength of ~0.8 Pa is found, which is comparable to commercial SLS powder [83] and spherical and dry coated polymer microspheres obtained by alternative approaches [17,19,23]. By dry coating the particle surface roughness is increased, which leads to an overall reduction of the interparticulate forces [32,84].

The powder deposition behavior, which is directly connected to the tensile strength and powder flowability [17,22], was assessed by doctor blading. In the powder deposition

experiment the application of a new powder layer in the SLS process is mimicked. The dry coated PC microspheres (T ≈ 240°C, n = 250 rpm, cooling without stirring) show superior deposition behavior (Figure 9): homogeneous powder layers with almost complete surface area coverage are obtained. The correlation between improved flowability and increasing substrate coverage in the deposition experiment is confirmed [17].

The influence of powder properties on SLS is also reflected by produced thin layer specimen depicted in Figure 10. For uncoated spherical PC microparticles only porous, fragmented layers were obtained (Figure 10 a), whereas dense sintered layers could be built with dry coated spherical PC microparticles. Figures 10 b to 10 d show the influence of the scan speed on the layer quality. For a scan speed v_{Laser} of 400 mm/s at constant laser power P = 20 W, decomposition of the polymer took place (c.f. color change), i.e. the laser energy input (see eq. 3) was too high. If the scan speed was too high (at constant laser power) energy input was insufficient to completely fuse the powder and only fragile layers were obtained. Optimum results with respect to layer quality at a laser power of 20 W were obtained for a scan speed of 600 mm/s.

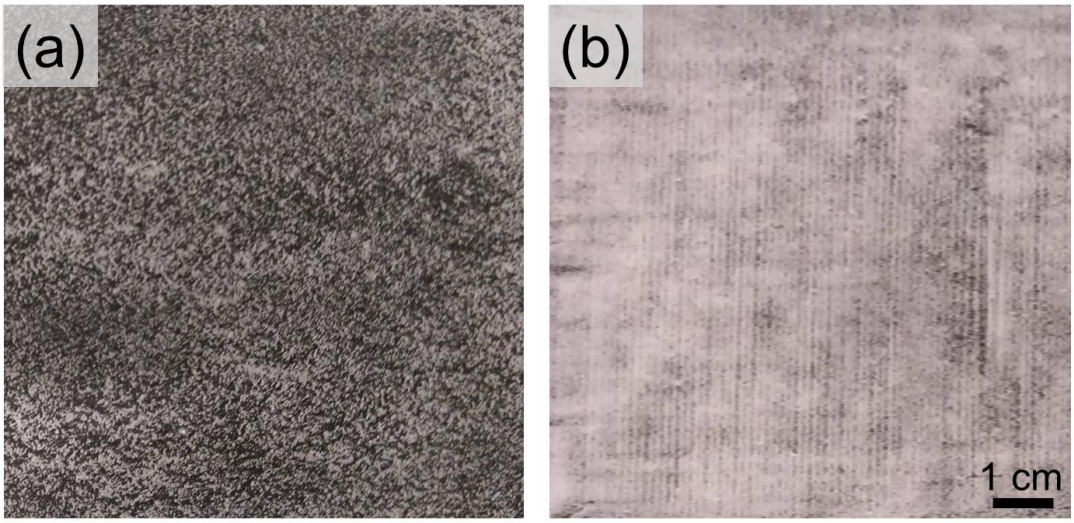

Figure 9: Powder deposition behavior of (a) spherical PC particles and (b) spherical, dry coated PC microspheres.

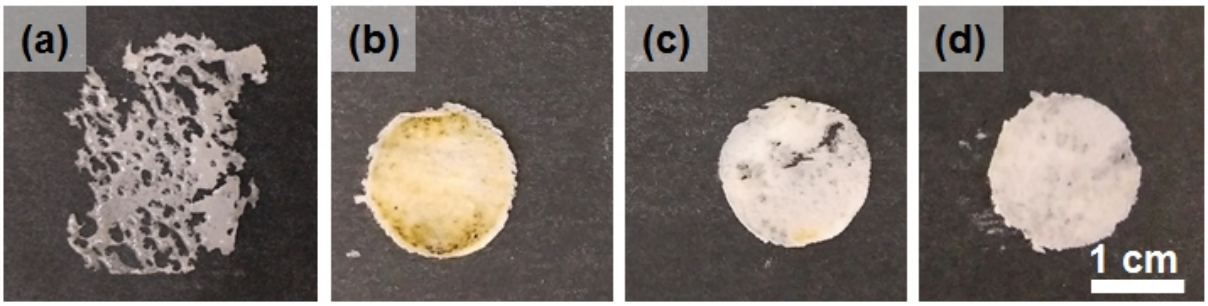

Figure 10: Thin layer specimen obtained by selective laser sintering (P = 20 W, D_{Laser} = 0.2 mm) out of (a) spherical PC particles (v_{Laser} = 500 mm/s) and (b-d) spherical and dry coated PC particles produced with different scan speeds ((b) v_{Laser} = 400 mm/s, (c) v_{Laser} = 500 mm/s and (d) v_{Laser} = 600 mm/s).

Conclusions

Spherical semi-crystalline polycarbonate (PC) micro particles of a size $x_{50,3}$ between 10 to 30 microns and narrow size distribution were produced by thermally induced liquid-liquid phase separation (TIPS) from commercially available amorphous PC granules. The temperature for complete dissolution and the cloud point of the system were measured. A process temperature larger than 144°C to 148°C depending on the system composition is necessary to completely dissolve the polymer and to subsequently induce TIPS. The product particle size depends on the temporal evolution of process temperature, mixing and the polymer concentration in the system. Especially stirring and choice of the maximum process temperature allow tailoring the product particle size: With increasing stirring speed and stirring during cooling the particle sized decreases; increasing the process temperature leads to larger particles. The product morphology can be tuned by choice of the polymer concentration: almost perfect spherical particles were observed for a PC concentration of 1 wt-%, whereas cauliflower-shaped particles were found at 3 wt-% PC. For larger polymer concentrations (> 5 wt-%) porous membranes are formed, i.e. only rather dilute conditions lead to particles in the PC - cyclohexanol system. The proposed straightforward TIPS approach is scalable, i.e. it can be transferred to plant scale for production.

The produced particles are semi-crystalline as proven by DSC, XRD and Raman spectroscopy. The degree of crystallinity could be varied in the range between 18 % (process temperature: 240°C) and 34 % (165°C) by choice of the maximum process temperature. After melting the obtained solid is completely amorphous like the initial PC feed material. Semi-crystallinity will be beneficial for the SLS process; it allows for higher building chamber temperatures in SLS and utilization of the thermal ‘sintering window’, which is not possible for amorphous PC. After dry coating with fumed silica the flowability of the PC particles

remarkably improved, as demonstrated by tensile strength measurements and powder deposition experiments.

The obtained composite PC powder were successfully employed to build dense thin layer specimen at appropriate SLS machine settings, which is a first step towards demonstration of SLS processability of this novel powder system. The correlation between particle properties (shape, surface roughness), flowability and specimen quality also is confirmed in the present case; powders of good flowability are a prerequisite for SLS.

Acknowledgements

This study has been supported by Deutsche Forschungsgemeinschaft (DFG) in the framework of the collaborative research center SFB 814 “Additive Manufacturing” (project A1 and A3). Financial support is gratefully acknowledged. The authors thank Tanja Bosch for assistance with preparing the thin layer specimen.

Symbols

c_{PC}	Polycarbonate concentration	/ wt%
D_{Laser}	Laser spot diameter	/ mm
ΔH_f	Melting enthalpy	/ J/g
ΔH_f^0	Melting enthalpy of fully crystalline PC	/ J/g
E	Laser energy input per beam area	/ J/mm^2
K	1st Mark–Houwink parameter	/-
M	Molar mass	/ g/mol
n	Stirrer speed	/ 1/min
n_P	Pin rotor speed	/ 1/min
P	Laser power	/ W
t	Temperature holding time	/ min
T	Temperature	/ °C
T_g	Glass transmission temperature	/ °C
T_m	Melting point	/ °C
T_{set}	Set temperature on heating plate	/ °C
v_{Laser}	Scan speed	/ mm/s
x	Particle size	/ µm
X_c	Crystallinity	/ %

Greek letters

λ	Wavelength	/ m
ρ	Density	/ g/cm^3
θ	Angle of diffraction	/ °

Supporting information

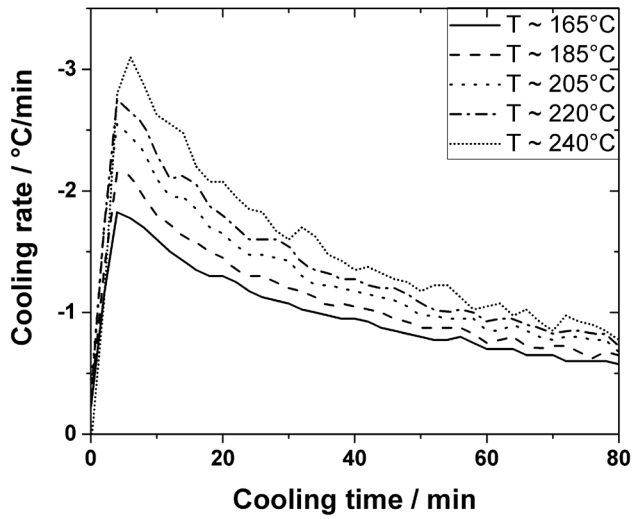

Figure S-1: Cooling rates for different maximum temperatures for the first 80 min of cooling.

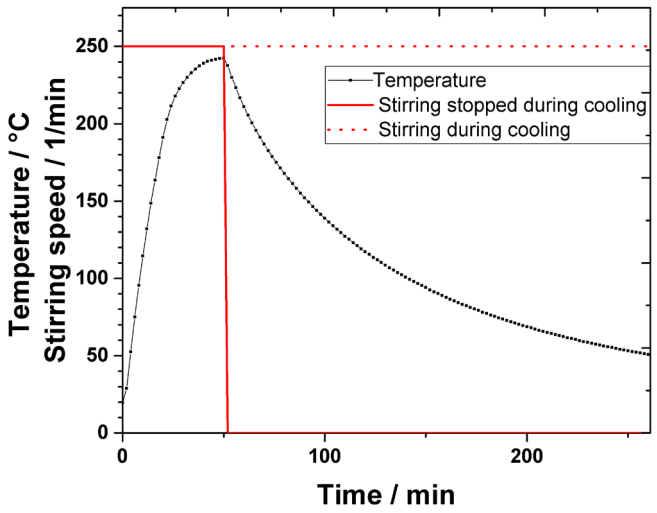

Figure S-2: Temperature and stirring profile for autoclave experiments shown for T ≈ 240 °C and n = 250 rpm (— without stirring during cooling, - - - with stirring during cooling)

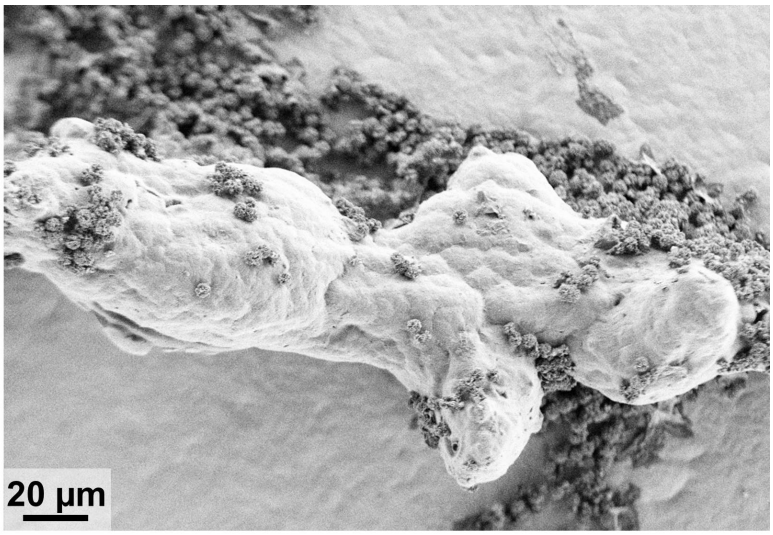

Figure S-3: SEM images of produced polycarbonate micro structures obtained by a process temperature of 144°C: pre ground feed material and small particles produced by TIPS coexisted due to an insufficient solving behavior of PC in cyclohexanol at lower temperatures.

Literature

[1] M. Schmid, Selektives Lasersintern (SLS) mit Kunstoffen - Technologie, Prozesse und Werkstoffe, Carl Hanser Verlag, München, 2015.

[2] T. Wohlers, Wohlers Report 2014 - 3D Printing and Additive Manufacturing - State of the Industry, Wohlers Associates, Inc., 2014.

[3] R.D. Goodridge, C.J. Tuck, R. Hague, Laser sintering of polyamides and other polymers, Progress in Materials Science 57 (2012) 229–267.

[4] H.F. Mark, Encyclopedia of polymer science and technology, Wiley-Interscience, Hoboken, N.J., 2007.

[5] G.V. Salmoria, J.L. Leite, C. Lopes, R. Machado, A. Lago, The manufacturing of PMMA/PS blends by selective laser sintering, Proceedings of the 3rd International Conference on Advanced Research in Virtual and Rapid Prototyping (2007) 305–311.

[6] G.V. Salmoria, J.L. Leite, L.F. Vieira, A. Pires, C. Roesler, Mechanical properties of PA6/PA12 blend specimens prepared by selective laser sintering, Polymer Testing 31 (2012) 411–416.

[7] J. Schmidt, S. Romeis, W. Peukert, Production of PBT/PC Particle Systems by Wet Grinding, AIP Proceedings in press (2017).

[8] G.V. Salmoria, J.L. Leite, C.H. Ahrens, A. Lago, A. Pires, Rapid manufacturing of PA/HDPE blend specimens by selective laser sintering: Microstructural characterization, Polymer Testing 26 (2007) 361–368.

[9] J. Scheirs, T.E. Long, Modern Polyesters: Chemistry and Technology of Polyesters and Copolyesters, John Wiley & Sons, Inc, Southern Gate, Chichester, West Sussex, 2005.

[10] J.C. Nelson, S. Xue, J.W. Barlow, J.J. Beaman, H.L. Marcus, D.L. Bourell, Model of the selective laser sintering of bisphenol-A polycarbonate, Industrial & Engineering Chemistry Research 32 (1993) 2305–2317.

[11] K.M. Fan, W.L. Cheung, I. Gibson, Movement of powder bed material during the selective laser sintering of bisphenol-A polycarbonate, Rapid Prototyping Journal 11 (2005) 188–198.

[12] H. Ho, I. Gibson, W. Cheung, Effects of energy density on morphology and properties of selective laser sintered polycarbonate, Journal of Materials Processing Technology 89–90 (1999) 204–210.
[13] J. Bertling, C. Eloo, Verdichtetes Kohlendioxid als Prozessadditiv zur Herstellung polymerer und mikronisierter Nanocomposite : Abschlussbericht zum FuE-Projekt: „nanocrosser“, 01th ed., 2008.
[14] M. Wilczek, J. Bertling, D. Hintemann, Optimised technologies for cryogenic grinding, Special Issue Supplement Comminution 2002 74, Supplement (2004) S425-S434.
[15] M. Wolff, S. Antonyuk, S. Heinrich, G.A. Schneider, Attritor-milling of poly(amide imide) suspensions, Particuology 17 (2014) 92–96.
[16] M. Schäfer, V.T. Kemtchou, U.A. Peuker, The grinding of porous ion exchange particles, Powder Technology 291 (2016) 14–19.
[17] J. Schmidt, M. Sachs, S. Fanselow, M. Zhao, S. Romeis, D. Drummer, K.-E. Wirth, W. Peukert, Optimized polybutylene terephthalate powders for selective laser beam melting, Chemical Engineering Science 156 (2016) 1–10.
[18] J. Schmidt, M. Plata, S. Tröger, W. Peukert, Production of polymer particles below 5 µm by wet grinding, Powder Technology 228 (2012) 84–90.
[19] J. Schmidt, M. Sachs, C. Blümel, B. Winzer, F. Toni, K.-E. Wirth, W. Peukert, A novel process route for the production of spherical LBM polymer powders with small size and good flowability, Powder Technology 261 (2014) 78–86.
[20] S. Ziegelmeier, P. Christou, F. Wöllecke, C. Tuck, R. Goodridge, R. Hague, E. Krampe, E. Wintermantel, An experimental study into the effects of bulk and flow behaviour of laser sintering polymer powders on resulting part properties, Journal of Materials Processing Technology 215 (2015) 239–250.
[21] S. Dadbakhsh, L. Verbelen, T. Vandeputte, D. Strobbe, P. van Puyvelde, J.-P. Kruth, Effect of Powder Size and Shape on the SLS Processability and Mechanical Properties of a TPU Elastomer, Laser Assisted Net Shape Engineering 9 International Conference on Photonic Technologies Proceedings of the LANE 2016 September 19-22, 2016 Fürth, Germany 83 (2016) 971–980.
[22] C. Blümel, M. Sachs, T. Laumer, B. Winzer, J. Schmidt, M. Schmidt, W. Peukert, K.-E. Wirth, Increasing flowability and bulk density of PE-HD powders by a dry particle coating process and impact on LBM processes, Rapid Prototyping Journal 21 (2015) 697–704.
[23] S. Fanselow, S.E. Emamjomeh, K.-E. Wirth, J. Schmidt, W. Peukert, Production of spherical wax and polyolefin microparticles by melt emulsification for additive manufacturing, Chemical Engineering Science 141 (2016) 282–292.
[24] M. Sachs, M. Friedle, J. Schmidt, W. Peukert, K.-E. Wirth, Characterization of a downer reactor for particle rounding, Powder Technology (2017).
[25] J. Schmidt, M. Sachs, S. Fanselow, K.-E. Wirth, W. Peukert, Herstellung und Funktionalisierung neuartiger Pulverwerkstoffe für die additive Fertigung, Chemie Ingenieur Technik 88 (2016) 1208.
[26] M. Sachs, J. Schmidt, F. Toni, C. Blümel, B. Winzer, W. Peukert, K.-E. Wirth, Rounding of Irregular Polymer Particles in a Downer Reactor, New Paradigm of Particle Science and Technology Proceedings of The 7th World Congress on Particle Technology 102 (2015) 542–549.
[27] A. Baule, R. Mari, L. Bo, L. Portal, H.A. Makse, Mean-field theory of random close packings of axisymmetric particles, Nature communications 4 (2013) 2194.

[28] S. Haeri, Y. Wang, O. Ghita, J. Sun, Discrete element simulation and experimental study of powder spreading process in additive manufacturing, Powder Technology 306 (2017) 45–54.
[29] E.J. Parteli, T. Pöschel, Particle-based simulation of powder application in additive manufacturing, Powder Technology 288 (2016) 96–102.
[30] S. Haeri, Optimisation of blade type spreaders for powder bed preparation in Additive Manufacturing using DEM simulations, Powder Technology 321 (2017) 94–104.
[31] J. Yang, A. Sliva, A. Banerjee, R.N. Dave, R. Pfeffer, Dry particle coating for improving the flowability of cohesive powders, Prof. Dr.-Ing. Otto Molerus 70th birthdayCongratulations to Prof. Dr.-Ing. Otto Molerus on the occasion of his 70th birthday on June 18th 2004 158 (2005) 21–33.
[32] R. Pfeffer, R.N. Dave, D. Wei, M. Ramlakhan, Synthesis of engineered particulates with tailored properties using dry particle coating, Granulation and Coating of Fine Powders 117 (2001) 40–67.
[33] S.-J. Wang, J.-Y. Liu, L.-Q. Chu, H. Zou, S.-J. Zhang, C.-J. Wu, Preparation of polypropylene microspheres for selective laser sintering via thermal-induced phase separation: Roles of liquid–liquid phase separation and crystallization, J. Polym. Sci. Part B: Polym. Phys. 55 (2017) 320–329.
[34] M.E. Nichols, R.E. Robertson, Preparation of small poly(butylene terephthalate) spheres by crystallization from solution, J. Polym. Sci. B Polym. Phys. 32 (1994) 573–577.
[35] S. Mumcu, H. Winzer, Verfahren zur Herstellung von pulverförmigen Beschichtungsmitteln auf der Basis von Polyamiden mit mindestens 10 aliphatisch gebundenen Kohlenstoffatomen pro Carbonamidgruppe, 1985.
[36] N. Wilczok, G. Dreske, F.-E. Baumann, Verfahren zur Herstellung von Polyamid-Feinstpulvern und deren Verwendung, 1996.
[37] F. Baumann, N. Wilczok, Herstellung von Polyamid-Fällpulvern mit enger Korngrössenverteilung und niedriger Porosität, 1998.
[38] K. Meyer, I. Zimmermann, Effect of glidants in binary powder mixtures, Powder Technology 139 (2004) 40–54.
[39] A. Schweiger, I. Zimmermann, A new approach for the measurement of the tensile strength of powders, Powder Technology 101 (1999) 7–15.
[40] C.A. Garber, P.H. Geil, Solution Crystallization of Poly-3,3-Bis(Chloromethyl)-Oxacyclobutane, Journal of Applied Physics 37 (1966) 4034–4040.
[41] P. Schaaf, B. Lotz, J.C. Wittmann, Liquid-liquid phase separation and crystallization in binary polymer systems, Polymer 28 (1987) 193–200.
[42] I.L. Hay, A. Keller, Polymer deformation in terms of spherulites, Kolloid-Zeitschrift und Zeitschrift für Polymere 204 (1965) 43–74.
[43] W.-H. Hou, T.B. Lloyd, A new technique for preparing monodisperse polymer particles, J. Appl. Polym. Sci. 45 (1992) 1783–1788.
[44] J.J. Blaker, J.C. Knowles, R.M. Day, Novel fabrication techniques to produce microspheres by thermally induced phase separation for tissue engineering and drug delivery, Acta Biomaterialia 4 (2008) 264–272.
[45] F.J. Tsai, J.M. Torkelson, The roles of phase separation mechanism and coarsening in the formation of poly(methyl methacrylate) asymmetric membranes, Macromolecules 23 (1990) 775–784.
[46] Z.-Y. Cui, C.-H. Du, Y.-Y. Xu, G.-L. Ji, B.-K. Zhu, Preparation of porous PVdF membrane via thermally induced phase separation using sulfolane, J. Appl. Polym. Sci. 108 (2008) 272–280.

[47] H. Matsuyama, M. Teramoto, S. Kudari, Y. Kitamura, Effect of diluents on membrane formation via thermally induced phase separation, Journal of Applied Polymer Science 82 (2001) 169–177.
[48] F.J. Hua, G.E. Kim, J.D. Lee, Y.K. Son, D.S. Lee, Macroporous poly(L-lactide) scaffold 1. Preparation of a macroporous scaffold by liquid–liquid phase separation of a PLLA–dioxane–water system, J. Biomed. Mater. Res. 63 (2002) 161–167.
[49] Y.S. Nam, T.G. Park, Porous biodegradable polymeric scaffolds prepared by thermally induced phase separation, Journal of biomedical materials research 47 (1999) 8–17.
[50] R.B. Richards, The phase equilibria between a crystalline polymer and solvents, Transactions of the Faraday Society 42 (1946) 10–28.
[51] P.J. Flory, Principles of polymer chemistry, Cornell University Press, Ithaca, London, 1953.
[52] B. Crist, A.R. Nesarikar, Coarsening in Polyethylene-Copolymer Blends, Macromolecules 28 (1995) 890–896.
[53] K.S. McGuire, A. Laxminarayan, D.R. Lloyd, Kinetics of droplet growth in liquid—liquid phase separation of polymer—diluent systems: Experimental results, Polymer 36 (1995) 4951–4960.
[54] P. van de Witte, P.J. Dijkstra, J. van den Berg, J. Feijen, Phase separation processes in polymer solutions in relation to membrane formation, Journal of Membrane Science 117 (1996) 1–31.
[55] F.J. Hua, G.E. Kim, J.D. Lee, Y.K. Son, D.S. Lee, Macroporous poly(L-lactide) scaffold 1. Preparation of a macroporous scaffold by liquid—liquid phase separation of a PLLA—dioxane—water system, Journal of biomedical materials research 63 (2002) 161–167.
[56] F. Gallez, R. Legras, J.P. Mercier, Some new aspects of the crystallization of bisphenol-A polycarbonate, Polymer Engineering & Science 16 (1976) 276–283.
[57] J.P. Kruth, X. Wang, T. Laoui, L. Froyen, Lasers and materials in selective laser sintering, Assembly Automation 23 (2003) 357–371.
[58] W. Feng, Z. Yin, W. Wang, L. Chen, X. Zhou, K. Qiu, J. Zhou, Y. Zhang, C. He, Synthesis and characterization of nanofibrous hollow microspheres with tunable size and morphology via thermally induced phase separation technique, RSC Adv 5 (2015) 61580–61585.
[59] T. Nie, M. He, M. Ge, J. Xu, H. Ma, Fabrication and structural regulation of PLLA porous microspheres via phase inversion emulsion and thermally induced phase separation techniques, J. Appl. Polym. Sci. 134 (2017) n/a-n/a.
[60] H. Schubert, Emulgiertechnik: Grundlagen, Verfahren und Anwendungen, 2nd ed., Behr‘s Verlag, Hamburg, 2010.
[61] H. Matsuyama, M. Teramoto, M. Kuwana, Y. Kitamura, Formation of polypropylene particles via thermally induced phase separation, Polymer 41 (2000) 8673–8679.
[62] C.A. Smolders, J.J. van Aartsen, A. Steenbergen, Liquid-liquid phase separation in concentrated solutions of non-crystallizable polymers by spinodal decomposition, Kolloid-Zeitschrift und Zeitschrift für Polymere 243 (1971) 14–20.
[63] J.M. Jonza, R.S. Porter, High-melting bisphenol-A polycarbonate from annealing of vapor-induced crystals, Journal of Polymer Science Part B: Polymer Physics 24 (1986) 2459–2472.
[64] G.E. Wissler, B. Crist, Glass transition in semicrystalline polycarbonate, Journal of Polymer Science: Polymer Physics Edition 18 (1980) 1257–1270.
[65] R.A. Ware, S. Tirtowidjojo, C. Cohen, Diffusion and induced crystallization in polycarbonate, J. Appl. Polym. Sci. 26 (1981) 2975–2988.

[66] S.M. Aharoni, N.S. Murthy, Effects of Solvent-induced Crystallization on the Amorphous Phase of Polycarbonate of bisphenol A), International Journal of Polymeric Materials and Polymeric Biomaterials 42 (1998) 275–283.
[67] H. Mochizuki, T. Mizokuro, N. Tanigaki, T. Hiraga, N. Tanaka, Crystallization of Bisphenol-A Polycarbonate by Using Vapor Transportation Methods, Polymer Journal 35 (2003) 535–538.
[68] E. Laredo, M. Grimau, A. Müller, A. Bello, N. Suarez, Influence of aging and crystallinity on the molecular motions in bisphenol-A polycarbonate, Journal of Polymer Science: Part B Polymer Physics 34 (1996) 2863–2879.
[69] J.P. Mercier, G. Groeninckx, M. Lesne, Some aspects of vapor-induced crystallization of polycarbonate of bisphenol A, Journal of Polymer Science Part C: Polymer Symposia 16 (1967) 2059–2067.
[70] F. Gallez, R. Legras, J.P. Mercier, Crystallization of bisphenol-A polycarbonate. I. Influence of trimellitic acid tridecyloctyl ester on the kinetics of crystallization, Journal of Polymer Science: Polymer Physics Edition 14 (1976) 1367–1377.
[71] Y. Sun, M. Matsumoto, M. Haruki, S.-i. Kihara, S. Takishima, Molecular weight dependence of the crystallization of the polycarbonate induced by supercritical CO2, The Journal of Supercritical Fluids 113 (2016) 144–149.
[72] X. Hu, A.J. Lesser, Enhanced crystallization of bisphenol-A polycarbonate by nano-scale clays in the presence of supercritical carbon dioxide, Polymer 45 (2004) 2333–2340.
[73] X. Liao, J. Wang, G. Li, J. He, Effect of supercritical carbon dioxide on the crystallization and melting behavior of linear bisphenol A polycarbonate, J. Polym. Sci. B Polym. Phys. 42 (2004) 280–285.
[74] H.R. Schubach, B. Heise, Structure and anisotropy in polycarbonate. I. Short range order of amorphous polycarbonate revealed by WAXS, Colloid and Polymer Science 264 (1986) 335–342.
[75] R.A. Ware, C. Cohen, Strain effects in the mass flux of methanol in poly(methyl methacrylate), J. Appl. Polym. Sci. 25 (1980) 717–729.
[76] B. von Falkai, W. Rellensmann, Kristallisation von Polycarbonaten. I. Lichtmikroskopische Untersuchungen, Makromol. Chem. 75 (1964) 112–121.
[77] T.G. Fox, P.J. Flory, Second-Order Transition Temperatures and Related Properties of Polystyrene. I. Influence of Molecular Weight, Journal of Applied Physics 21 (1950) 581–591.
[78] K. Hatzius, Y. Li, M. Werner, B.-J. Jungnickel, Phase diagram and crystallization of polycarbonate/poly-ϵ-caprolactone blends, Die Angewandte Makromolekulare Chemie 243 (1996) 177–187.
[79] X. Chang, T. Ding, H. Tian, T. Wang, Antisolvent crystallization and solid-state polymerization of bisphenol-A polycarbonate, Journal of Applied Polymer Science 133 (2016) n/a-n/a.
[80] J. Dybal, P. Schmidt, J. Baldrian, J. Kratochvíl, Ordered Structures in Polycarbonate Studied by Infrared and Raman Spectroscopy, Wide-Angle X-ray Scattering, and Differential Scanning Calorimetry, Macromolecules 31 (1998) 6611–6619.
[81] D.G. LeGrand, J.T. Bendler, Handbook of Polycarbonate Science and Technology, Marcel Dekker Inc., New York, Basel, 2000.
[82] B. Stuart, P. Thomas, Xylene swelling of polycarbonate studied using Fourier transform Raman spectroscopy, Spectrochimica Acta Part A: Molecular and Biomolecular Spectroscopy 51 (1995) 2133–2137.

[83] W. Kniffka, M. Eichmann, G. Witt (Eds.), Proceedings of the 13th Rapid.Tech Conference Erfurt, Germany, 14-16 June 2016: Prozessangepasste Charakterisierung der Fließfähigkeit pulverförmiger Strahlschmelzmaterialien, Hanser, München, 2016.
[84] H. Rumpf, Die Wissenschaft des Agglomerierens, Chemie Ingenieur Technik 46 (1974) 1–11.